arXiv:cond-mat/0312105v1 [cond-mat.soft] 3 Dec 2003

A quasi-local measure of inter-scale transfer: An approach to understanding turbulence

M.K. Rivera,[1,2] W.B. Daniel,[1,2] S.Y. Chen,[2,3] and R.E. Ecke[1,2]

[1]*Condensed Matter & Thermal Physics Group,Los Alamos National Laboratory, Los Alamos, NM 87545*
[2]*Center for Nonlinear Studies, Los Alamos National Laboratory, Los Alamos, NM 87545*
[3]*Department of Mechanical Engineering, The Johns Hopkins University, Baltimore, MD 21218*

(Dated: February 2, 2008)

Many questions remain in turbulence research—and related fields—about the underlying physical processes that transfer scalar quantities, such as the kinetic energy, between different length scales. Measurement of an ensemble-averaged flux between scales has long been possible using a variety of techniques, but instantaneous, spatially-local realizations of the transfer have not. The ability to visualize scale-to-scale transfer as a field quantity is crucial for developing a clear picture of the physics underlying the transfer processes and the role played by flow structure. A general technique for obtaining these scale-to-scale transfer fields, called the filter approach, is described. The effects of different filters, finite system size, and limited resolution are explored for experimental and numerical data of two-dimensional turbulence.

PACS numbers: 47.27-i

I. INTRODUCTION

Turbulence is characterized by the transfer of an inviscid constant, such as kinetic energy or a passive scalar, between different length scales. One of the primary goals of turbulence research is to understand the mechanisms that drive this transfer process. Numerical simulations performed by Farge *et al.* suggest that in both two-dimensional (2D) and three-dimensional (3D) turbulence it is a relatively small number of "coherent structures" that dominate the turbulent dynamics.[1,2] As a result, it is important to understand how the existence and interaction of these coherent structures affect the transfer processes. Thus, the *spatially-local* transfer properties of the flow need to be measured and correlated with these structures.

In this manuscript a tool for obtaining local information about the scale-to-scale transfer of inviscid constants from experimental/numerical data is examined. The method, called the "filter approach" (FA), has traditionally been applied to large-eddy numerical simulations (LES),[3] but is developed here in the context of experimental data analysis. By applying a low-pass spatial filter to the equations of motion (the incompressible Navier-Stokes equation), separate equations for the filtered, or large-scale, fields and the remaining small-scale fields can be derived.[4] Within the resulting equations are coupling terms that represent the interaction of the large- and small-scale fields with each other. In LES schemes the coupling terms in the large-scale equations are modeled thereby eliminating the necessity of directly computing the small scales.[3] In our application of the filter approach, however, data from direct numerical simulations (DNS) or high resolution experiments are used to directly evaluate the coupling terms and obtain a quasi-local measure of the inter-scale transfer.[5,6]

For readers familiar with LES and turbulence modeling it should be stressed that the philosophy driving our use of the filter approach is different from the *a priori* development of LES models discussed in.[7] There the objective was to determine empirically which of several LES modeling schemes for the large- to small-scale coupling terms most successfully emulates physical data. In that case, FA was used primarily as a benchmark, and only went as far as measuring the inter-scale coupling term. Rather than producing results for numerical benchmarking, FA can also be used as an analysis probe to determine where and when in a flow scale-to-scale transfer of inviscid constants takes place. In this way one can isolate important interaction events and form an understanding of turbulence inter-scale transfer mechanisms. Of course, this understanding could eventually be incorporated into LES models.

The filter approach is applied in this paper to both experimental and numerical data. The intent is not to investigate the underlying physics of the turbulence, which will be presented in later papers, but rather to determine the appropriate interpretation of the results and the limitations imposed by different filters, spatial boundaries, and finite measurement resolution.

II. EXPERIMENTAL AND NUMERICAL SYSTEMS

Experimental measurements were carried out in a flowing soap-film channel, a quasi-2D system in which decaying turbulence of low to moderate Reynolds number can be generated ($10^2 \leq Re \leq 10^4$). The channel was 5 cm wide and was inclined at an angle of 75° with respect to vertical. The mean flow was 120 cm/s and the film thickness was about 10 μm. A more detailed description of the channel can be found in.[8,9] Using the empirical relationships measured in,[10] the films' kinematic viscosity was $\nu \approx 0.03$ cm^2/s. The turbulence generating grid consisted of rods of 0.12 cm diameter with 0.22

cm spacing between the rods. Thus, the blocking fraction is around 0.3, which is typical for turbulence in 2D soap film flows.[8,11,12,13] The resulting Reynolds number, $Re = UL/\nu$, was 880 based on the mean-flow velocity and an injection scale of $L_{\rm inj} = 0.22$ cm. The turbulent velocity, $\mathbf{u}(\mathbf{x})$, and vorticity, $\omega(\mathbf{x})$, fields generated by the grid were obtained by tracking $3-5$ μm polystyrene spheres (density approximately 1.05 g/cc) within a 1.8×1.8 cm^2 region located 6 cm downstream from the grid (20-30 eddy rotation times).[14,15] The particles were illuminated with a double pulsed Nd:Yag laser and their images captured by a 12-bit, 2048×2048 pixel camera. Around 3×10^4 particles were individually tracked for each image pair and their velocities and local shears were interpolated to a discrete 135×135 grid. One-thousand velocity and vorticity fields were obtained in this way and were used to compute ensemble averages of the statistical measures described below. Typical velocity and vorticity fields are shown in Fig. 1.

To supplement the experimental data, a direct numerical simulation of the 2D Navier Stokes equation was performed. Computational details are presented in.[16] The equation

$$\frac{\partial \omega}{\partial t} + u_j \frac{\partial \omega}{\partial x_j} + \nu_m (-1)^m \frac{\partial^{2m} \omega}{\partial x_j^{2m}} = F \qquad (1)$$

was simulated in a square domain with side $L = 2\pi$ and periodic boundary conditions. Here, u_i is the i-th component of the velocity; $\omega = \epsilon_{ij} \partial_j u_i$ is the vorticity; and F is a stirring force applied to wave numbers $|\mathbf{k}| = 4 \rightarrow 7$. The Einstein summation convention is used throughout. Two values of m are considered: $m = 1$ corresponding to Laplacian viscosity ($\nu_1 = 0.01$), and $m = 8$ corresponding to hyper-viscosity ($\nu_8 = 1.4 \times 10^{-7}$), which has the effect of extending the inertial range.

The equation was solved using a fully de-aliased, parallel pseudo-spectral code with second-order Adam-Bashforth time-stepping. The resolution was 2048^2. A statistically-stationary state was achieved after about 200 large-eddy turn-over times. Representative examples of vorticity fields generated using Laplacian and hyper-viscosity are shown in Fig. 2.

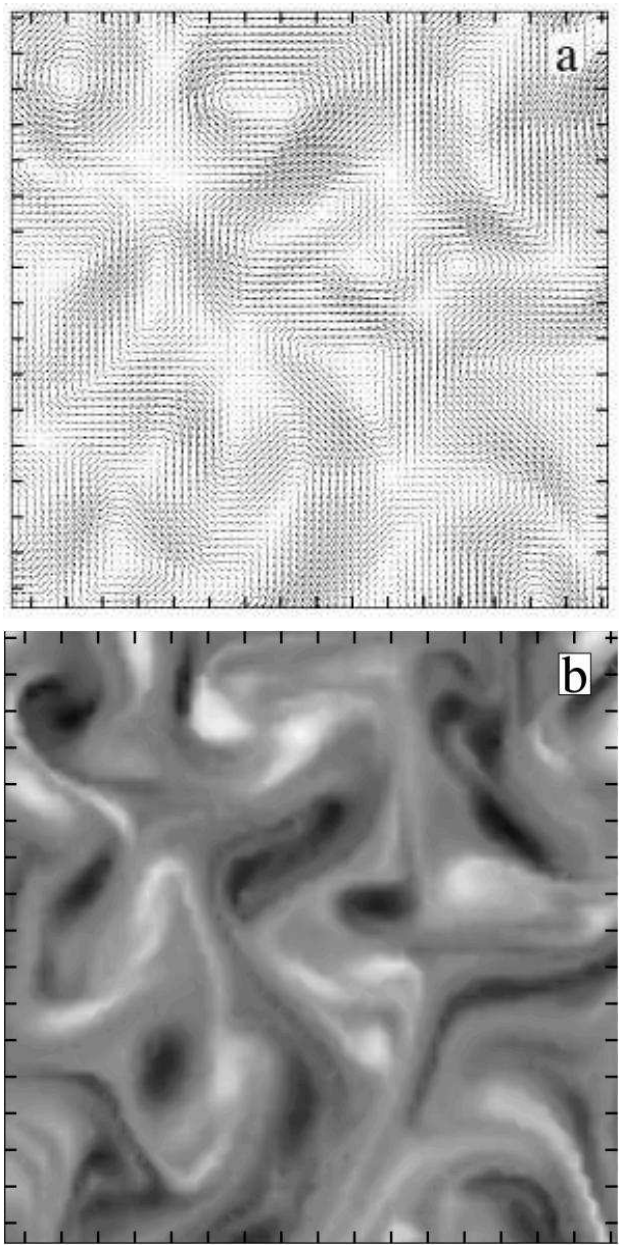

FIG. 1: Typical a) velocity and corresponding b) vorticity field obtained from the flowing soap film channel. The hash marks represent 1 mm increments, the mean flow (subtracted out) is in the $-\hat{y}$ direction. The top of the image is ≈ 3 cm downstream from the energy injection grid.

III. THE FILTER APPROACH

A. General Application

The filter approach allows the direct measurement of the coupling between scales in non-linear systems. It was originally developed as a tool to truncate numerical simulations of turbulence by modeling small-scale behavior with the knowledge of large-scale behavior, *i.e.* LES.[3] In this paper, the general application of FA to nonlinear systems will be considered first, followed by a specific example: the case of energy and enstrophy transfer between length scales in 2D turbulence.

General features of the transfer process are examined by considering a field, $q(\mathbf{x})$, that is evolved by a nonlinear evolution operator, $F^{(\rm nl)}$, as $F^{(\rm nl)} q = 0$. Given a scale, l, one can separate the field, q, into large-scale, q_l, and small-scale, q_s, components. This is done by convolving a filter function, G_l, with q and defining $q_l \equiv G_l * q$ and $q_s \equiv q - q_l = (\delta - G_l) * q$, where δ is the Dirac delta function. Applying G_l to the evolution equation for q yields $G_l * (F^{(\rm nl)} q) = 0$. Adding zero, written as

$F^{(\mathrm{nl})}q_l - F^{(\mathrm{nl})}q_l$, results in:

$$F^{(\mathrm{nl})}q_l = -(G_l * (F^{(\mathrm{nl})}q) - F^{(\mathrm{nl})}q_l). \quad (2)$$

Eq. (2) indicates that the large-scale field, q_l, evolves in exactly the same manner as the full field, q, up to a coupling term $C(q_l, q) \equiv -(G_l * (F^{(\mathrm{nl})}q) - F^{(\mathrm{nl})}q_l)$. This coupling term, which can be considered as an external forcing or damping, arises from the small-scale field, q_s, interacting with q_l. Thus, C provides a measure of the interaction between large and small scales. The measurement of C requires no assumptions about the field, q, such as homogeneity or isotropy. Moreover, C is a *field* quantity, not simply an average, and can reveal not only information about the coupling between scales, but also when and where such interactions are taking place and with what strength.

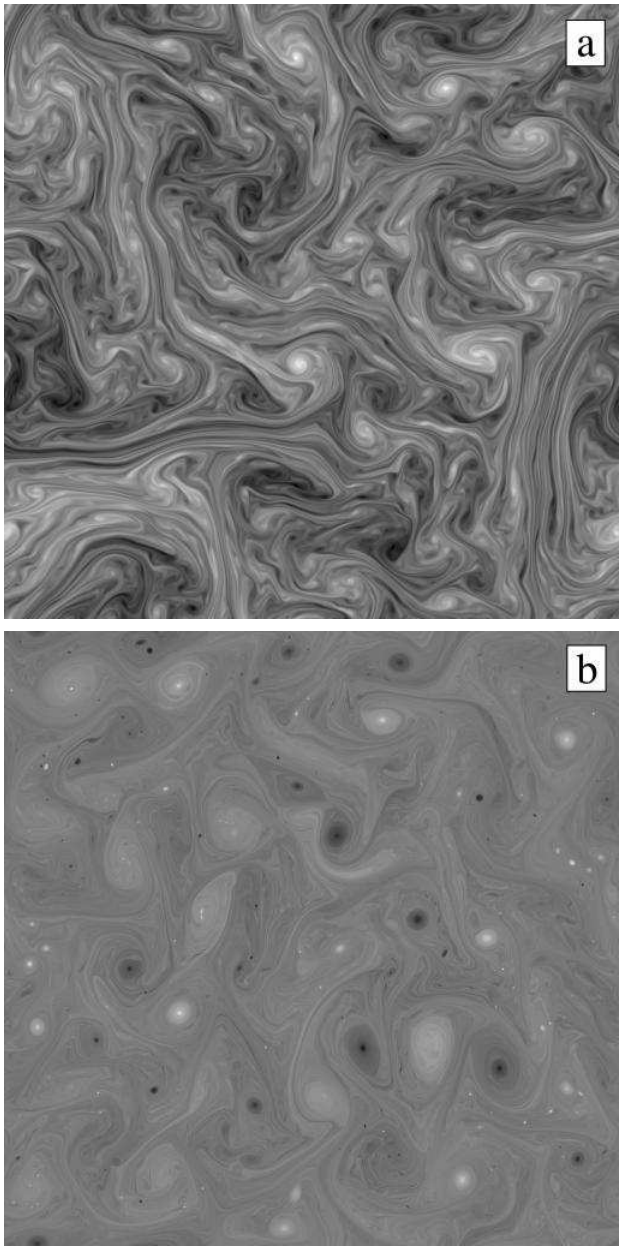

FIG. 2: DNS vorticity fields with a) Laplacian viscosity ($m = 1$) and b) hyper-viscosity ($m = 8$)

The field nature of the coupling term derived above, C, makes FA very valuable in the context of studying turbulence. As mentioned in the introduction, turbulence is characterized by an average scale-to-scale flux of quantities such as the kinetic energy. Many possible mechanisms underlying the transfer processes have been suggested, *e.g.*, the stretching of vortex tubes into thin filaments may account for some fraction of the down-scale transfer of energy in 3D.[17] In 2D, vortex merger has been postulated as a way of transferring energy to larger scales.[3] The difficulty is that neither of these pictures has been conclusively correlated with topological flow structures or the underlying transfer dynamics, though some attempts have been made.[18] By using FA to measure the inter-scale transfer and correlating this field with the position of flow structures (identified by other means), one can determine the veracity of these hypothesized transfer mechanisms.

There are a number of subtleties to consider when applying FA to experimental data. First, there is the choice of the filter function, G_l. The interpretation of the scale-to-scale transfer depends on the selection of the filter function. For example, if the convolution function is Gaussian defined by length scale l, the interpretation of the filtered functions is as given above. On the other hand, if the convolution is with the kernel $H_l \equiv (\delta - G_l)$, where again G_l is Gaussian and δ is a Dirac delta function, the resulting interpretation of the convolved fields, $H_l * f$, as "large-scale" is incorrect. Indeed, the function H_l produces "small-scale" fields. Other ramifications of changing the filter function will be explored shortly but the convention is adopted that the filter function is always low-pass.

Two additional considerations when applying FA to real data are finite measurement resolution and the existence of spatial boundaries. The extent to which the measurements are sensitive to either of these factors depends on the quality of the data and on the form of the filter used. Significant research in the context of LES has addressed similar concerns, but always for the purpose of approximating the physical system in a numerical simulation.[3] These issues are explored in some depth in a later section.

B. Application to two-dimensional turbulence: energy and enstrophy transport

In two-dimensional turbulence kinetic energy, $E \equiv u^2/2$, and enstrophy, $\Omega \equiv \omega^2/2$, are conserved in the inviscid limit. Theory, numerics, and experiments all indicate that energy is transferred on *average* from small to large length scales (up-scale) and that enstrophy is transferred in the opposite direction (down-scale).[19] FA, how-

ever, can be used to obtain much more detailed information about the energy and enstrophy transfer within the flow. We begin by examining the scale-to-scale coupling of energy in the 2D Euler equation (viscous terms are linear and, hence, cause no direct scale-to-scale transfer, eliminating the need to examine the full Navier-Stokes equation):

$$\frac{\partial u_i}{\partial t} + u_j \frac{\partial u_i}{\partial x_j} = -\frac{\partial p}{\partial x_i}, \tag{3}$$

where u_i is the i-th component of the velocity field, p is the density normalized pressure field, and summation over repeated indices is assumed. Contracting this evolution equation with a filter function, G_l, and extracting the coupling term as described above yields:

$$\begin{aligned} \frac{\partial (u_i)_l}{\partial t} &+ (u_j)_l \frac{\partial (u_i)_l}{\partial x_j} \\ &= -\frac{\partial p_l}{\partial x_i} - \frac{\partial}{\partial x_j}((u_i u_j)_l - (u_i)_l (u_j)_l). \end{aligned} \tag{4}$$

The notation $(f)_l$, or simply f_l, will be used to denote the large-scale field $G_l * f$. Eq. (4) is almost the equivalent of Eq. (2). The one delicacy is that the term p_l is not the large-scale pressure field, *i.e.*, it is not the field obtained using the gradients of $(u_i)_l$. This is not an important issue here, however, because, as will be demonstrated later, p_l does not contribute to the inter-scale transfer.

From Eq. (4) the scale-to-scale coupling term for the velocity is given by

$$C((u_i)_l, u_i) = -\frac{\partial \tau_{ij}^{(l)}}{\partial x_j}, \tag{5}$$

where $\tau_{ij}^{(l)} = (u_i u_j)_l - (u_i)_l (u_j)_l$ is the subgrid-scale stress tensor. To obtain the equation for the evolution of large-scale energy, $E^{(l)} = (u_i)_l^2/2$ one multiplies Eq. (4) by $(u_i)_l$. (Note that the notation $E^{(l)}$ is used rather than E_l since $E_l = (u_i^2)_l/2 \neq (u_i)_l^2/2 = E^{(l)}$.) The resulting equation,

$$\frac{\partial E^{(l)}}{\partial t} + \frac{\partial}{\partial x_j}((u_j)_l E^{(l)} + (u_j)_l p_l) = -(u_i)_l \frac{\partial \tau_{ij}^{(l)}}{\partial x_j}. \tag{6}$$

for the energy contained at scales larger than l, is identical to the full energy evolution equation up to the coupling term on the right hand side (again ignoring the pressure term).

This coupling term is not yet in the form to directly yield scale-to-scale energy transfer information. There are two ways in which the small-scale velocities can change the large-scale energy: by physically transporting it from point-to-point or by transferring it between scales. To separate the two, the Leibnitz rule is used to rewrite the right hand side of Eq. (6) as

$$= -\frac{\partial}{\partial x_j}((u_i)_l \tau_{ij}^{(l)}) + \tau_{ij}^{(l)} \frac{\partial (u_i)_l}{\partial x_j}. \tag{7}$$

Notice that the latter of these two terms is Galilean invariant, whereas the former is not. Boosts to the reference frame should not change the scale-to-scale transfer of energy but will change the point-to-point transport. Therefore, the former term is attributed to the point-to-point transport and the latter to the scale-to-scale transfer.

Another way to contrast the point-to-point coupling with scale-to-scale coupling is to consider the limit of a homogenous system. In this case taking an ensemble average, $\langle \ldots \rangle$, should eliminate all point-to-point transport terms, leaving only inter-scale transfer contributions. Since the action of ensemble averaging commutes with the derivative operation, and since the spatial derivative of an ensemble average is zero in the limit of homogeneity, the ensemble average of Eq. (6) is simply $\partial_t \langle E^{(l)} \rangle = \langle \tau_{ij}^{(l)} \partial_j (u_i)_l \rangle$. Not only does this demonstrate that $\partial_j [\tau_{ij}^{(l)} (u_i)_l]$ is a point-to-point term, but it also demonstrates that all of the terms on the left, other than the time derivative, are point-to-point as well. This fact allows us to ignore the delicacy with respect to the pressure term: it does not affect scale-to-scale transfer.

For simplicity Eq. 6 is rewritten as

$$\frac{\partial E^{(l)}}{\partial t} + \frac{\partial J_j^{(l)}}{\partial x_j} = -\Pi^{(l)}, \tag{8}$$

where $J_j^{(l)}$ and $\Pi^{(l)}$ are defined as

$$J_j^{(l)} \equiv (u_j)_l E^{(l)} + (u_i)_l \tau_{ij}^{(l)} + (u_j)_l p_l, \tag{9}$$

$$\Pi^{(l)} \equiv -\tau_{ij}^{(l)} \frac{\partial (u_i)_l}{\partial x_j} = -\tau_{ij}^{(l)} (S_{ij})_l. \tag{10}$$

where $(S_{ij})_l$ is the large-scale strain tensor. The negative sign in the definition of $\Pi^{(l)}$ is added so that down-scale transfer has a positive value whereas up-scale transfer is negative.

An almost identical method can be used to determine the scale-to-scale enstrophy transfer of the flow. The starting point, however, is the 2D Euler equation for vorticity,

$$\frac{\partial \omega}{\partial t} + u_j \frac{\partial \omega}{\partial x_j} = 0. \tag{11}$$

As above, the equation is contracted with a filter function, G_l, and the coupling term is extracted,

$$\frac{\partial \omega_l}{\partial t} + (u_j)_l \frac{\partial \omega_l}{\partial x_j} = -\frac{\partial \sigma_j^{(l)}}{\partial x_j}, \tag{12}$$

where $\sigma_j^{(l)} = (u_j \omega)_l - (u_j)_l \omega_l$ is the subgrid scale vorticity transport vector. Notice that the term $\sigma_j^{(l)}$ defined in Eq. 12 has an almost identical form to $\tau_{ij}^{(l)}$ in the energy equations. This general form is typical of the filter

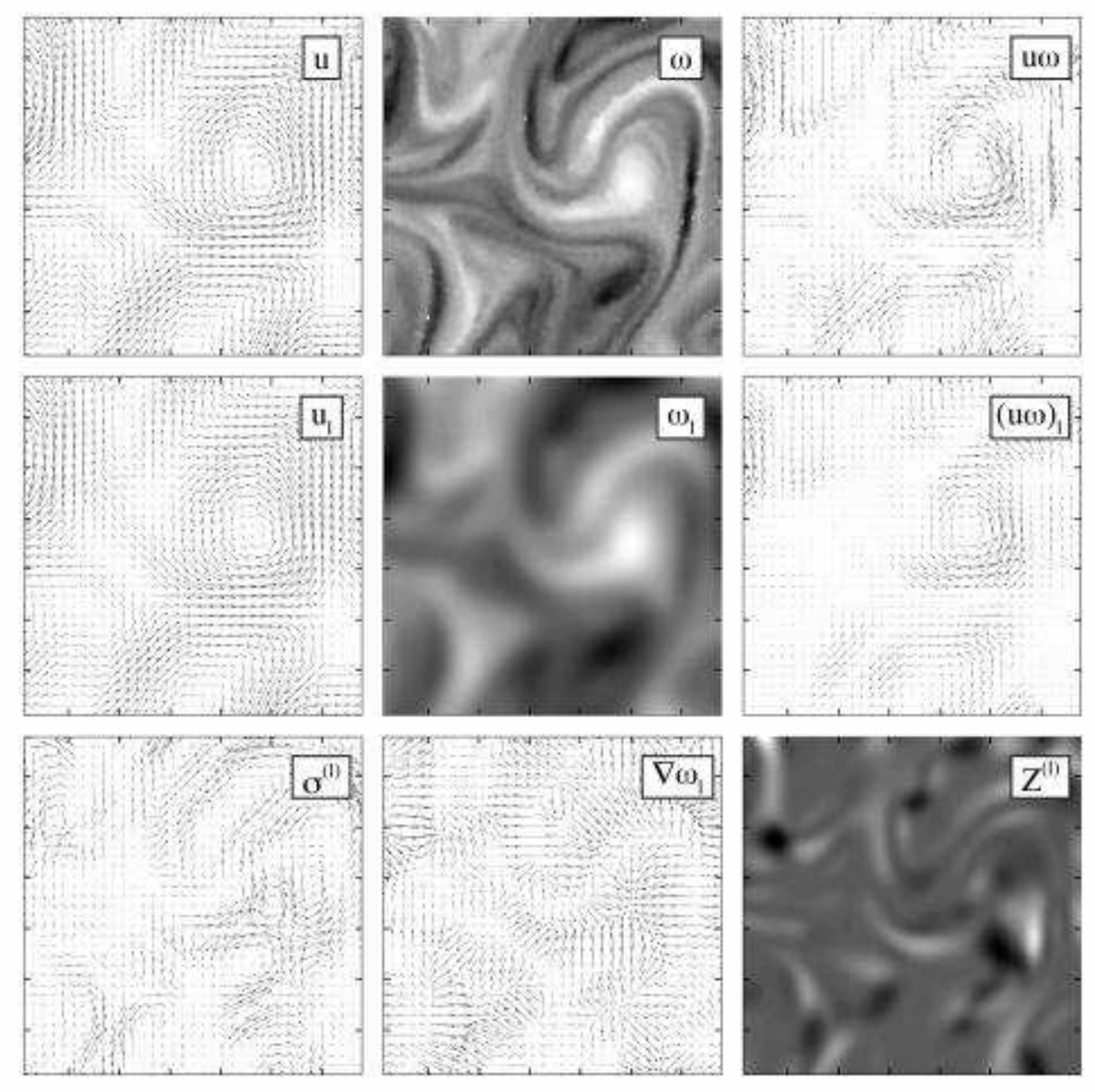

FIG. 3: Obtaining the scale-to-scale enstrophy flux $Z^{(l)}$ for a velocity field obtained from the soap film. The filter function, G_l, used was Gaussian with $l = 0.2$ cm. Row 1: Unfiltered velocity, $\mathbf{u}$, vorticity, ω, and vorticity transport $\mathbf{u}\omega$. Row 2: Filtered velocity, $\mathbf{u}_l$, vorticity, ω_l, and vorticity transport, $(\mathbf{u}\omega)_l$. Row 3: The subgrid vorticity transport vector $\sigma^{(l)}$, large scale vorticity gradient $\nabla\omega_l$ and the scale-to-scale enstrophy transfer $Z^{(l)}$.

approach. The coupling terms between large- and small-scale fields often take the form $(ab)_l - a_l b_l$ for quadratic nonlinearities.

To change the large-scale vorticity equation to an equation for large-scale enstrophy evolution, one must multiply by ω_l. This yields

$$\begin{aligned}\frac{\partial \Omega^{(l)}}{\partial t} &+ \frac{\partial}{\partial x_j}((u_j)_l \Omega^{(l)}) = -\omega_l \frac{\partial \sigma_j^{(l)}}{\partial x_j} \\ &= -\frac{\partial}{\partial x_j}(\omega_l \sigma_j^{(l)}) + \sigma_j^{(l)} \frac{\partial \omega_l}{\partial x_j}, \end{aligned} \tag{13}$$

where again the Leibniz rule was used to separate point-

to-point transport from inter-scale transfer. Grouping the appropriate terms, as was done for the energy equation, leads to the final form,

$$\frac{\partial \Omega^{(l)}}{\partial t} + \frac{\partial K_j^{(l)}}{\partial x_j} = -Z^{(l)}, \tag{14}$$

where

$$K_j^{(l)} \equiv (u_j)_l \Omega^{(l)} + \sigma_j^{(l)} \omega_l \tag{15}$$

$$Z^{(l)} \equiv -\sigma_j^{(l)} \frac{\partial \omega_l}{\partial x_j} \tag{16}$$

where the negative sign in front of the scale-to-scale coupling term, $Z^{(l)}$, again makes down-scale transfer positive.

To make the above derivations more concrete, some examples are provided of filtered fields. For purposes of illustration, vorticity and enstrophy fields are presented and an analysis of velocity and energy fields is left to a later publication. Figure 3 displays steps in the calculation of the scale-to-scale enstrophy transfer, $Z^{(l)}$, for a typical vorticity field extracted from experimental data. For this calculation the filter function was a Gaussian with Fourier-space definition

$$G_l(\mathbf{k}) = \mathbf{e}^{-\frac{|\mathbf{k}|^2}{\mathbf{k_l^2}}}, \tag{17}$$

where $k_l \equiv 2\pi/l$. These figures illustrate that the application of FA is straightforward: (1) compute the secondary field, $u_i\omega$, from the measured velocity and vorticity fields; (2) perform a convolution of these fields to obtain $\sigma_i^{(l)}$; (3) take the scalar product of $\sigma_i^{(l)}$ with the appropriate gradient of the large-scale fields, namely $\partial_i \omega_l$.

There is, however, a caveat for the general case. It may not always be possible to separate the point-to-point transport from the scale-to-scale transfer terms. For the energy equation, the terms were determined by using the Leibniz rule to separate out the Galilean invariant part of the energy flux. For the enstrophy, the separation was obtained by analogy with the energy equation rather than by a strict application of Galilean invariance. There is no *a priori* expectation that such a separation will be as simple, or even possible, for arbitrary nonlinear systems. In compressible flows, for example, it is possible to measure the coupling terms, but the point-to-point transport caused by small scales is tied to the scale-to-scale transfer in a non-trivial way. The interpretation of such results must, therefore, be done carefully.

IV. SYSTEMATIC EFFECTS

This section will address the effect of varying the filter, G_l, on the interpretation of the results, the consequences of the data being limited in spatial extent (*i.e.* by boundaries), and variations in the results caused by experimental or numerical limitations on the resolution of the data.

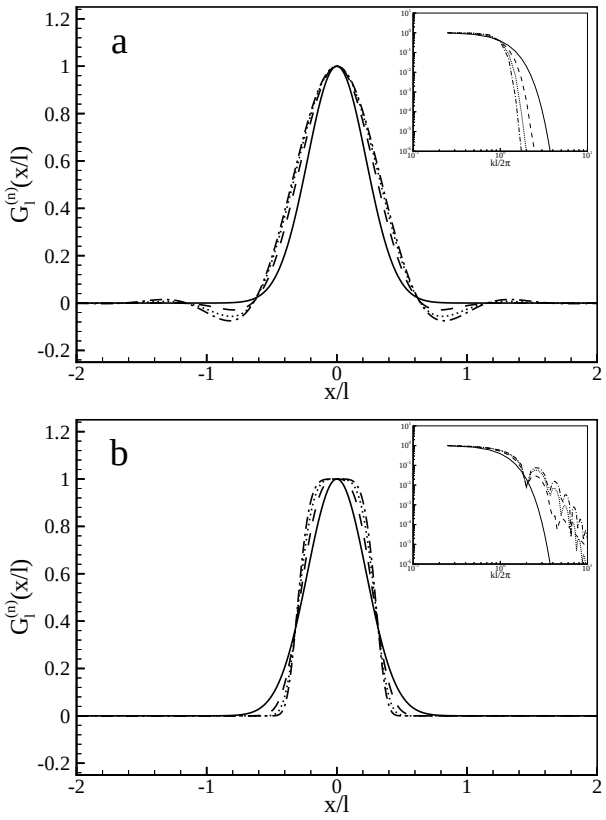

FIG. 4: Illustration of the various filter functions $G_l^{(n)}$ that are used in the paper (see Eq. 18 and Eq. 19 for details) For both plots the real space convolution function is presented with the root of the Fourier spectrum inset. (a) Fourier filter convolution kernels, for orders n=2 (solid), n=3 (dash), n=4 (dotted), n=5 (dash-dot). (b) Real space filters for orders n=2 (solid), n=3 (dash), n=4 (dotted),n=5 (dash-dot).

A. Different Filters

The interpretation of the results of FA may depend on the form of the filter function, G_l. A Gaussian kernel was used in Eq. (17), but this particular choice was made only because it has a simple interpretation in both real- and Fourier-space, taking the same form in both. The FA technique imposes no such constraints in general. In some cases, one may want to preferentially constrain the filter in real-space to a well-defined length scale or, instead, may want to filter so as to select only a sharp band of wave numbers. Either possibility can be explored using this tool. It must be kept in mind, however, that sharpening the filter in real- or Fourier-space causes a corresponding broadening of the filter in the other. The impact and interpretation of varying the form of the filter on the resulting fields is considered here.

The form of the Fourier filters used is

$$G_l^{(n)}(\mathbf{k}) = \mathbf{e}^{-\left(\frac{|\mathbf{k}|}{\mathbf{k_l}}\right)^n}, \tag{18}$$

where n is the filter order. The case $n = 2$ is the Gaus-

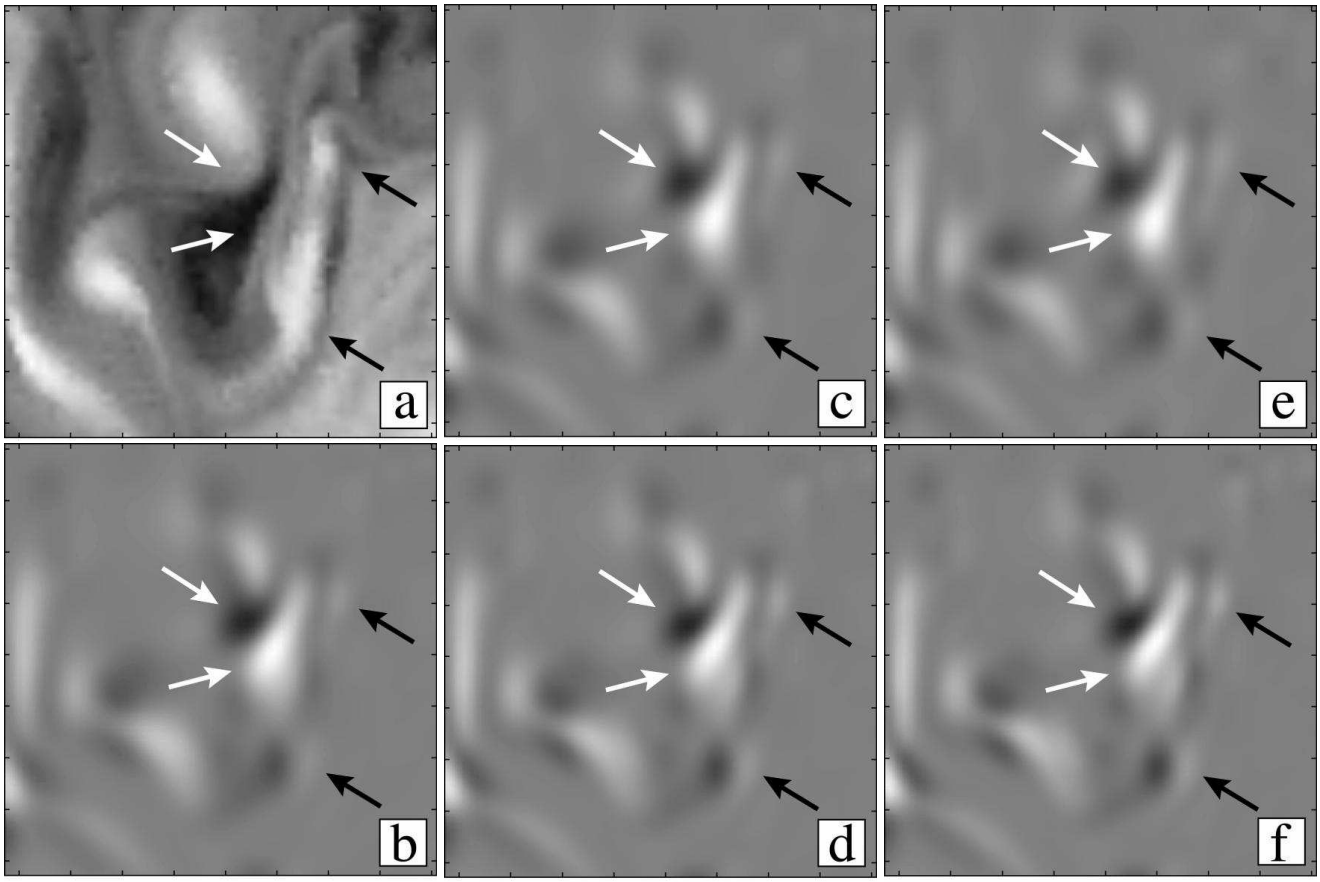

FIG. 5: (a) Subsection of a typical vorticity field obtained from the soap film. (b)-(f) Calculation of $Z^{(l)}$ from vorticity field shown in (a) using $l = 0.15$ cm and various Fourier and real space filters. (b) Gaussian filter (grayscale range $\pm 1.95 \times 10^7 \mathrm{s}^{-3}$) (c) Fourier filter of order $n = 3$ (grayscale range $\pm 2.47 \times 10^7 \mathrm{s}^{-3}$) (d) Real filter of order $n = 3$ (grayscale range $\pm 1.93 \times 10^7 \mathrm{s}^{-3}$) (e) Fourier filter of order $n = 4$ (grayscale range $\pm 2.83 \times 10^7 \mathrm{s}^{-3}$) (f) Real filter of order $n = 4$ (grayscale range $\pm 1.90 \times 10^7 \mathrm{s}^{-3}$). The hatch marks represent 1 mm increments.

sian filter considered earlier. As n increases, the filter sharpens around the Fourier mode corresponding to filter length l. Similarly, the real-space filters are defined by:

$$G_l^{(n)}(\mathbf{x}) = \mathbf{A}\mathbf{e}^{-\left(\frac{|\mathbf{x}|}{l/\pi}\right)^n}. \tag{19}$$

Note that for $n = 2$, the real filter is equivalent to the Fourier filter. As the real filter is sharpened it approaches an area average over a box of diameter $2l/\pi$. Both of these sets of filters are shown in Fig. 4. Other types of filter are possible, but are not considered here.

From an experimental point of view, the sharper real-space filters are more attractive than the Fourier filters because the real-space envelope of the Fourier filters grows as the order of the filter is increased. Since experimental data is invariably windowed to the cross-section of the measurement apparatus, this means that sharper Fourier filters quickly grow to interact with boundaries. For sharp real filters this is not a problem: as the filter increases in sharpness it becomes more spatially compact. For the purpose of comparing with theory, however, sharper Fourier filters approach the ideal; see, for example, the discussion given in Frisch[17] in which the fields are filtered by an infinitely sharp cutoff in Fourier-space.

In Fig. 5, the results of using a Gaussian, two low-order Fourier-space filters, and two low-order real-space filters in the calculation of the enstrophy transfer are shown (the associated vorticity field is also displayed). Superficially, the fields are fairly similar. The strength of the fluctuations, however, changes with filter (the grey scale limits of the fields are noted in the captions). The change in magnitude is stronger for Fourier filters than real-space filters, with the $n = 4$ Fourier-space filter experiencing 50% larger fluctuations than for $n = 2$.

The similarity in the fields seems to indicate that the *relative* magnitudes of enstrophy flux remain more or less constant. In particular, the stronger values of flux associated with powerful vortices (middle top and middle left) have almost identical forms, though there may be a slight sharpening of the lobes for both higher order real-space and Fourier-space filters (which, we note, have a quadrupolar form). Higher-order Fourier-space filters increase the symmetry of many features, *i.e.* they appear

less ovular (see for example the lobes indicated by the white arrows in Fig. 5), whereas the contrast between features and the background is enhanced by higher-order real-space filters. On the whole, however, the qualitative features are fairly insensitive to the form of filter used, maybe surprisingly so. One might expect that the beating of the sharper Fourier kernel in real space would show up more strongly in the fields. For the stronger enstrophy transfer signals this does not appear to be the case.

Weaker signals are more sensitive to the particular choice of filter. Consider the weak lobe in the lower middle of the field indicated by the black arrow in Fig. 5 (or the one in the middle right also indicated by a black arrow). For the Gaussian filter, the lobe is barely visible. For sharper filters in both real- and Fourier-space ($n = 4$), however, the prominence of this lobe with respect to the stronger signals in the system is enhanced.

The most important observation is that the qualitative structure of the field is relatively unaffected by the choice of filter. Sharper filters increase the "contrast", but neither eliminate nor create structural features in the flow. For the purposes of correlating scale-to-scale transfer to topological features, this is an important feature of FA.

The above comparison is only qualitative. A more accurate quantitative comparison is presented in Fig. 6, where the probability distribution function of the enstrophy transfer is presented for the same set of filters used in Fig. 5. The agreement between the different filters is quite good, but a little deceptive. Note, first, that the magnitude of the RMS fluctuations has been normalized out. Second, there may be (though it is, perhaps, below the noise level) a slight increase in asymmetry, in particular in the negative tail of the PDF for real-space filters (the open symbols). Given that in Fig. 5 the large values of enstrophy transfer, corresponding to the tails of the PDF, are relatively insensitive to changes in the filter, this collapse of the PDFs is reasonable.

On the other hand, in Fig. 5 the weaker values of inter-scale transfer have somewhat increased contrast. This change is emphasized in the lowest-order moments of the distribution, rather than in the tails. The average, $\langle Z^{(l)} \rangle$, and fractional sign-probability comparison, $\delta P(Z^{(l)}) \equiv P(Z^{(l)} > 0) - P(Z^{(l)} < 0)$, are shown in Fig. 7. Here, there is a significant difference in the average enstrophy flux as a function of filter order. In particular, the average rises and falls more sharply for the higher-order Fourier-space filters than it does for the real-space filters. Also, the area fraction saturates at a smaller value, then falls more quickly. The signs of the average flux and the area difference, however, are quite robust, although the magnitudes seem to vary (in some places by a factor of two over this range of filter orders). The rise in the peak of average scale-to-scale transfer is reminiscent of ringing such as takes place in the Gibbs phenomenon. It is not clear whether or not this is the source of the change.

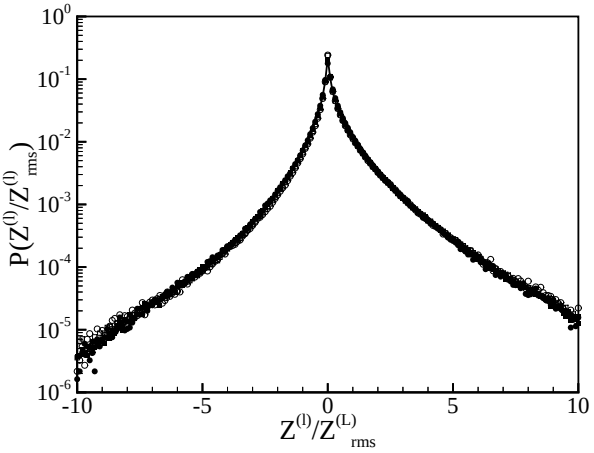

FIG. 6: The probability distribution function (normalized by RMS) for $Z^{(l)}$ obtained using a Gaussian (solid line) two Fourier-space filters of order $n = 3$(solid squares) and $n = 4$ (solid circles) and two real-space filters of order $n = 3$(open squares) and $n = 4$ (open circles). The filter length was $l = 0.2$ mm.

1. *Interpretation*

At this point, one might ask: for which filter is the result closest to the "real" enstrophy flux? This question depends entirely on what one means by "enstrophy flux". The scale-to-scale transfer between wave numbers is most closely approximated by higher-order Fourier filters. Because of the associated broadening of the filter in real-space, however, the resulting fields are not as good a measure of the spatially-local enstrophy transfer. On the other hand, for the flux to be localized in physical space for comparison with real-space structures, sharp real-space filters are preferable. In this limit, the enstrophy flux can no longer be defined as the movement of enstrophy from small Fourier modes to larger ones but is actually a measure of the flux out of some bands and into others (which do not necessarily have larger wave number). The strength of FA does not lie in its ability to measure *the exact magnitude of the transfer*, but rather that the sign of the transport and the qualitative form of the fields is robust to changes in the filter.

B. Boundaries

An important consideration when using FA, one that is also a major issue in LES, is the presence of boundaries (either physical or as limits of the viewing window). As a Fourier-space filter grows in order, and correspondingly in real-space extent, less and less of the data can be used as the boundaries begin to affect the computation of the convolution in regions farther and farther into the interior.

To investigate the influence of finite system size a ran-

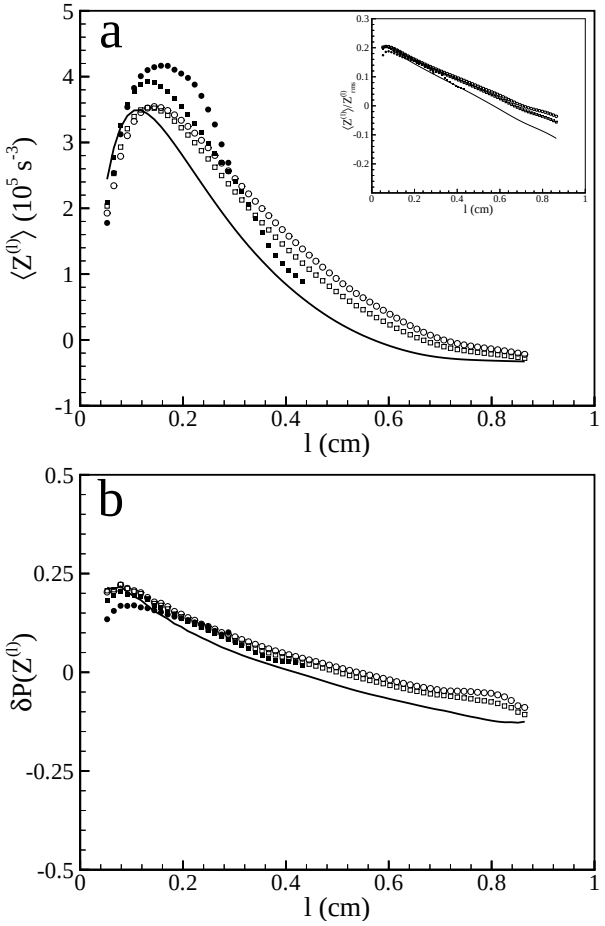

FIG. 7: (a) The average enstrophy flux $\langle Z^{(l)} \rangle$ and (b) $\delta P(Z^{(l)})$ (see text) for a range of length scales calculated using data from the soap film and a Gaussian filter function (solid line), two Fourier space filters of order $n = 3$(solid squares) and $n = 4$ (solid circles) and two real-space filters of order $n = 3$ (open squares) and $n = 4$ (open circles). Inset in (a) is the average fluxes normalized by the RMS fluctuation size for the respective filters.

dom periodic streamfunction was generated on a 512×512 grid. This streamfunction was then used to obtain velocity and vorticity fields from which the enstrophy flux field, $Z_0^{(l)}$, was computed. The left half of the fields was then set to zero and the enstrophy field, $Z_b^{(l)}$, recalculated. The normalized RMS difference,

$$Z_{\rm error}^{(l)} = \frac{\langle (Z_b^{(l)} - Z_0^{(l)})^2 \rangle^{1/2}}{(Z_0^{(l)})_{\rm RMS}}, \qquad (20)$$

is shown in Fig. 8 as a function of x/l, the distance from the introduced boundary normalized by the filter size. The various plots are given for Fourier-space filters of different orders (see Eq. 18).

With the exception of the order 3 filter there is a continuous increase in the boundary affects. Taking a nominal error rate of 10^{-4} as acceptable, a boundary of $b \approx l(n-1)$ is appropriately sized for the data. This

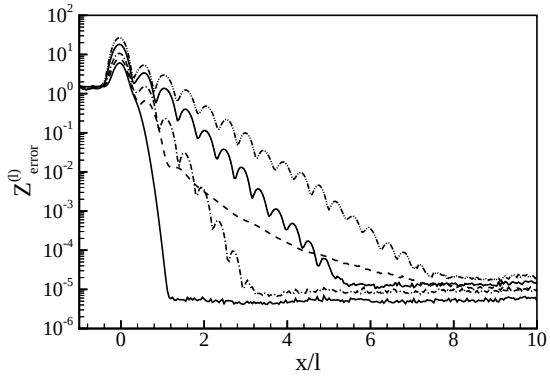

FIG. 8: Interaction of various order Fourier-space filters with a boundary at $x/l = 0$. The graphs denote the RMS difference between the enstrophy flux measured in the presence of a boundary and that without. The various curves are for a Gaussian filter (solid-line), and Fourier filters of order $n = 3$ (dashed), $n = 4$ (dash-dot), $n = 6$ (dotted), $n = 8$ (dash-dot-dot).

results in a loss of $2l(n-1)$ in linear box size since one must apply the condition to left-right (top-bottom) boundaries. This effective boundary has been adhered to throughout this paper. For real-space filters the boundaries become less of an issue. Indeed, for the sharpest real-space filter (a simple average over a circle), the boundary is $l/2$.

C. Effects of Finite Resolution

In this section the effect of finite measurement resolution on the ability of FA to resolve the behavior of the enstrophy flux for a given filter function is explored. In the preceding sections experimental data was used in the analysis, but to estimate the effects of finite resolution it is necessary to consider numerical data where the range of scales and the uncertainty in the measured values is fairly well known. The numerical data also eliminates any concerns about the effect of boundaries since the boundary conditions are periodic.

Pre-filtering at the limit of the data resolution should result in no apparent difference in the transfer from that computed from the original field. As the pre-filter length, L, is increased above the resolution scale differences in the measured transfer will increase. The question this raises is: how far above L are these finite-resolution effects felt? To answer this question a series of $20^{\rm th}$ order real-space filters with varying L are applied to two data sets simulating the local averaging inherent in experimental measurements (such as image acquisition and particle tracking). From these pre-filtered fields the enstrophy transfer, $Z_L^{(l)}$, is calculated and compared with the full flux.

The results of these calculations are shown for both

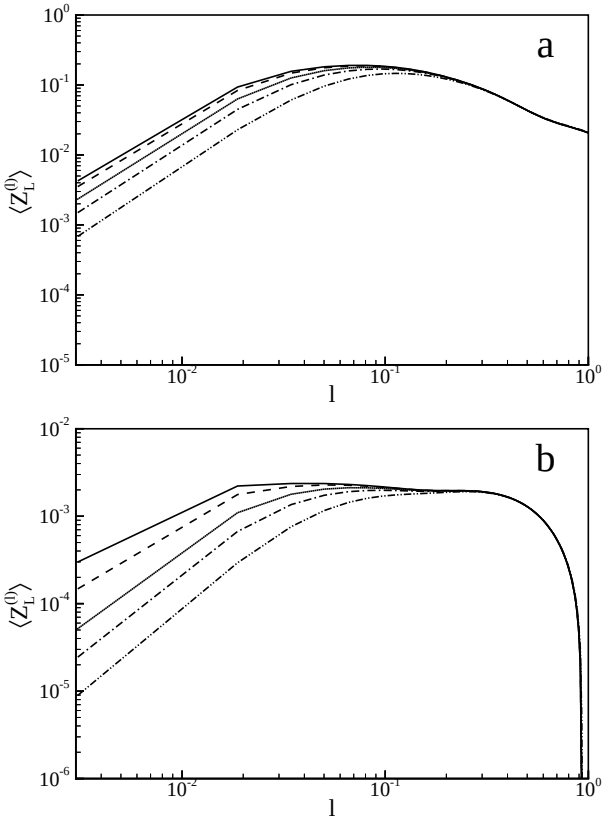

FIG. 9: The average enstrophy flux calculated using numerical data for (a) Laplacian viscosity and (b) hyper-viscosity with a pre-filter of length $L = 0.01$ (dashed), 0.02 (dotted), 0.03 (dash-dot), 0.05 (dash-dot-dot). Also displayed is the total enstrophy flux (solid line) in the simulations.

data sets in Fig. 9. For both, the viscous cut-off scale is between 0.01 and 0.02. For pre-filters with L at or below this length there is little change in the magnitude of the average flux (slightly more prominent in the case of hyper-viscosity). Once the filter size exceeds the viscous scale, *i.e.*, penetrates at all into the inertial range, the effects are quickly felt up to almost the injection scale, 0.4. This may be a general feature of FA, or it may be a peculiarity of the 2D enstrophy transfer process being non-local. In either case, it demonstrates the importance of resolving the entire inertial range, including the viscous scale, for an accurate representation of the enstrophy transfer to be possible. Whether or not enstrophy transfer is local in Fourier-space is an important question in its own right, and one which is sufficiently complex to warrant exploration in a separate paper.

V. CONCLUSIONS

In the above discussion and use of FA, familiar turbulence assumptions, such as homogeneity, isotropy, and inertial range, were not requirements of the measurement. This is perhaps the greatest strength of FA: it can be applied to any type of turbulent flow, regardless of that particular flow's properties. All that is needed is the evolution equation for the system from which the inter-scale transfer can be obtained. The flow doesn't have to be turbulent, FA can be applied to laminar or periodic flow and reasonable results obtained. In other words, the interpretation of FA *does not rely on a pre-existing theory*. Rather, it is a tool that can directly test notions of how inter-scale transfer takes place in systems and can be used to build appropriate theories.

This "bottom up" approach to physics (rather than a theoretical trickle down) comes at a price: one must have highly resolved fields of data with a significant range of spatial scales. The former is a requirement imposed by the resolution issues discussed above, which can only be relaxed if one assumes a wavenumber local inter-scale transfer process. The latter is a limitation imposed by the data windowing and interaction of the filters with the measurement boundary. Of course, the standard techniques of measuring velocity fields in fluids, namely particle imaging velocimetry or particle tracking, more or less ensure that the measurements are not far from the viscous scale, and thus of high enough resolution to not assume local transfer. This is because these techniques rely on groups of particles moving coherently, which only holds when the scales being probed are small enough that local Taylor expansions describe the flow. The difficulty is in simultaneously measuring a significant range of scales above the viscous scale for meaningful information to be obtained. With standard PIV practices this is possible in 2D. Only with holographic PIV is this possible in 3D. There, however, the limitation is in the amount of data that can be obtained (order 10 fields is possible; currently, 1000 fields are not).

As discussed in the introduction, our ultimate intention for the FA technique is to probe the mechanisms driving the inter-scale transfer in 2D turbulence, with a particular eye towards the role of coherent structures in the transfer process. This will be done both via statistical analysis of fields in the laboratory frame of reference (Eularian frame), as well as following the motion of fluid parcels (Lagrangian frame). FA, however, is not limited to these measurements alone, but could find application to the inter-scale transfer and mixing of passive scalars, or other quantities not necessarily conserved in the inviscid limit (*i.e.* local topology). And as hinted at previously, FA can be applied (carefully!!!) to general non-linear systems where an equation of motion is known and inter-scale transfer is of interest.

VI. ACKNOWLEDGMENTS

We thank Greg Eyink, Phil Marcus, Misha Chertkov and Boris Shraiman for interesting discussions and suggestions.

[1] M. Farge, K. Schneider, and N. Kevlahan, Physics of Fluids **11**, 2187 (1999).

[2] M. Farge, G. Pellegrino, and K. Schneider, Physical Review Letters **87**, 4501 (2001).

[3] M. Lesieur, *Turbulence in Fluids* (Kluwer Academic Publishers, 1987).

[4] M. Germano, Journal of Fluid Mechanics **238**, 325 (1992).

[5] B. Tao, J. Katz, and C. Meneveau, Journal of Fluid Mechanics **457**, 35 (2002).

[6] M. Rivera, W. Daniel, S. Chen, and R. Ecke, Physical Review Letters **90**, 4502 (2003).

[7] C. Menevau and J. Katz, Annual Review of Fluid Mechanics pp. 1–32 (2000).

[8] M. Rivera, P. Vorobieff, and R. Ecke, Physical Review Letters **81**, 1417 (1998).

[9] P. Vorobieff, M. Rivera, and R. Ecke, Physics of Fluids **11**, 2167 (1999).

[10] P. Vorobieff and R. Ecke, Physical Review E **60**, 2953 (1999).

[11] M. Gharib and P. Derango, Physica D **37**, 406 (1989).

[12] H. Kellay, X. Wu, and W. Goldburg, Physical Review Letters **74**, 3975 (1995).

[13] M. Rutgers, X. Wu, and W. Daniel, Review of Scientific Instruments **72**, 3025 (2001).

[14] M. Ishikawa, Y. Murai, and F. Yamamoto, Measurement Science Technology **11**, 677 (2000).

[15] K. Ohmi and H. Li, Experiments in Fluids **11**, 603 (2000).

[16] S. CHen, R. Ecke, G. Eyink, X. Wang, and Z. Xiao, Physical Review Letters (2003).

[17] U. Frisch, *Turbulence: The Legacy of A. N. Kolmogorov* (Cambridge University Press, 1995).

[18] W. Daniel and M. Rutgers, Physical Review Letters **89**, 4502 (2002).

[19] R. Kraichnan and D. Montgomery, Reports on Progress in Physics **43**, 547 (1980).